Accepted Manuscript

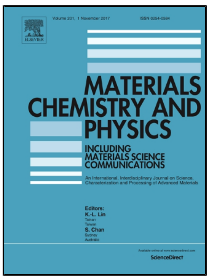

Effects of sintering temperature on microstructure and mechanical properties of spark plasma sintered titanium

Mehdi Shahedi Asl, Abbas Sabahi Namini, Amir Motallebzadeh, Maziyar Azadbeh

PII:	S0254-0584(17)30770-8
DOI:	10.1016/j.matchemphys.2017.09.069
Reference:	MAC 20036
To appear in:	*Materials Chemistry and Physics*
Received Date:	23 May 2017
Revised Date:	11 September 2017
Accepted Date:	29 September 2017

Please cite this article as: Mehdi Shahedi Asl, Abbas Sabahi Namini, Amir Motallebzadeh, Maziyar Azadbeh, Effects of sintering temperature on microstructure and mechanical properties of spark plasma sintered titanium, *Materials Chemistry and Physics* (2017), doi: 10.1016/j.matchemphys.2017.09.069

- Microstructure and mechanical properties of spark plasma sintered Ti were studied.
- Sintering process was performed at 750–1350 ºC for 5 min under 50 MPa in vacuum.
- A fully-dense sample with highest mechanical performance was obtained at 1200 ºC.

Effects of sintering temperature on microstructure and mechanical properties of spark plasma sintered titanium

Mehdi Shahedi Asl [a*], Abbas Sabahi Namini [b], Amir Motallebzadeh [c], Maziyar Azadbeh [d]

[a] *Department of Mechanical Engineering, University of Mohaghegh Ardabili, Ardabil, Iran*

[b] *Department of Engineering Sciences, Sabalan University of Advanced Technologies (SUAT), Namin, Iran*

[c] *Koc University Surface Science and Technology Center, Istanbul, Turkey*

[d] *Department of Materials Engineering, Sahand University of Technology, Tabriz, Iran*

*Corresponding Author:

M. Shahedi Asl Tel.: +989123277186 Email: shahedi@uma.ac.ir

Abstract

Titanium is a lightweight metal with particular properties which make it the material of choice for many different applications. Among powder metallurgy techniques, rapid manufacturing routes at relatively low temperatures, such as spark plasma sintering (SPS) process, which involve the simultaneous application of pressure and temperature, result in titanium engineering components with higher relative density and good mechanical properties, compared to the conventional sintering methods. The microstructure evolution and mechanical properties of spark plasma sintered commercially pure titanium were studied. Sintering process was performed at a temperature range of 750–1350 ºC for a dwell time of 5 min under an external pressure of 50 MPa in vacuum. The samples were investigated in terms of relative density, microstructure, phase analysis, tensile properties, bending strength, hardness and nanoindentation. Results were judgmentally discussed and associated to SPS temperature. A fully-dense sample with highest mechanical performance was obtained after SPS at 1200 ºC.

Keywords: Spark plasma sintering; Titanium; Microstructure; Mechanical properties; Nanoindentation.

1. Introduction

Titanium-based materials have an extraordinary combination of characteristics such as good mechanical properties (e.g. high temperature strength), biocompatibility and excellent corrosion resistance in many different aggressive environments which nominate them as one of the most favorable candidates for particular applications. However, processing of titanium to fabricate reliable parts, especially by powder metallurgy techniques, is extremely complicated and costly [1-5].

Compared to the conventional powder metallurgy routes for fabrication of near fully dense metals such as hot pressing, the spark plasma sintering is known as an excellent method which quickly produces the product at lower temperatures. Employing a short-time sintering process is helpful when a fine-grained microstructure is strongly demanded. In SPS process, a pulsed electric current is applied while an external load is coupled, after placing the powder in a graphite die. Then, material transfer and diffusion phenomena are accelerated because of plasma generation between the starting particles which leads to breakdown and cleaning of oxide impurities from the surface layers. Moreover, joule effect and pressure-assisted plastic deformation result in better densification and sinterability [6-10].

Eriksson et al. [11] rapidly densified coarse titanium powders (~45 μm) by SPS technique to obtain fully dense samples. The presence of pulsed electrical current had a positive effect on the densification process of titanium. Deformation was found as the dominant densification mechanism throughout the whole particles, particularly, in α-phase region. Zadra et al. [12] investigated the fabrication of commercially pure titanium (with two different powder grades) by SPS route at the temperature range of 700–1150 ºC for 5 min under 60 MPa. They confirmed that an excellent microstructural, chemical and mechanical properties is obtainable by spark plasma sintering at the temperature of 900 ºC.

Nanoindentation is known as an almost fully developed technique which employs the recorded penetration depth of an indenter into the sample together with the measured applied load to obtain some mechanical properties from the experimental load–displacement curve. For example, hardness, elastic modulus, strain hardening index, fracture toughness, yield strength and residual stress can be determined by nanoindentation

technique. The most important advantage of such test is its localization. Indeed, it can be performed on only one grain (submicron sized region) and the test can be repeated several times [13-17].

This work deals with the processing of titanium powder by means of spark plasma sintering at different temperature of 750, 900, 1050, 1200 and 1350 ºC for dwell time of 5 min under pressure of 50 MPa in vacuum atmosphere and aims at investigating the physical/mechanical properties and microstructural evolution with the sintering temperature. A review of the available literature shows that although several research works have been performed on SPS of titanium powders, but little specific investigations were found on the processing of titanium by SPS method and characterizing by nanoindentation technique.

2. Experimental procedure

2.1. Processing

In this study, commercially pure hydride–dehydride (HDH) Ti powder (particle size <75 µm, purity >98%) was purchased from Sigma-Aldrich company. SEM micrograph and XRD pattern of the as-received titanium powders are shown in Fig. 1. According to Fig. 1a, the morphology of powder particles is generally angular. The only detectable crystalline phase in the powder batch is titanium, based on the X-ray diffraction pattern presented in Fig. 1b. Chemical composition of the starting material is presented in Table 1.

A spark plasma sintering furnace (EF-SPS-20T-10) with a pulse duration of 3.3 ms and a current on-off ratio of 12:2 was used for sintering of the samples at different temperatures. Graphite dies, lined with thin flexible graphite foils as lubricant, were employed to fabricate disc–shaped samples (50 mm diameter and ~6 mm thickness). The temperature was monitored using an infrared thermocouple oriented towards a hole on the external wall of the die directly. The samples were spark plasma sintered at five designated temperatures of 750, 900, 1050, 1200 and 1350 °C with a heating rate of 50 °C/min through increasing the direct current. Applied external pressure during the sintering process was 50 MPa in vacuum condition of <1 Pa. Isothermal dwelling at the sintering temperature was 5 min.

2.2. Characterization

Bulk density was measured by the Archimedes technique with distilled water as the immersion medium. Theoretical density of titanium powder was supposed 4.45 g/cm^3, based on the supplier's datasheet. Relative density is the ratio of the measured density to the theoretical density. Conventional methods of grinding, polishing and etching (Krolls reagent: 5 ml HF, 10 ml HNO_3, 85 ml H_2O) were employed for surface preparation. Phase characterization of the as-received Ti powder and the polished surfaces of sintered bodies was fulfilled by XRD analysis (Siemens D5000, Cu lamp, λ=1.54 Å, 40 kV, 30 mA). Microstructures of the polished and fracture surfaces were studied by optical microscopy (PMG3, Olympus, Japan) and scanning electron microscopy (Cam Scan 2300, Czech Republic), respectively. Microhardness was measured by carrying out ten Vickers' indentation (Eseway, UK) on the polished surface of each sample with a load of 0.3 Kg for 15 s. For evaluation of mechanical properties, the samples were cut to standard dimensions by electrical discharge machining (EDM). Room temperature tensile strength and three-point bending strength were assessed by STM-250 universal testing machine at 0.5 mm/min constant crosshead speed. The sample dimensions for bending test were 3×4×34 mm^3 (according to ASTM B528) with a span of 15 mm. Tensile specimens have gauge dimensions of 2×5×15 mm^3 (according to ISO 6892-1:2016 and ASTM E8/E8M) and a total of three tests were done to obtain an average value of bending and tensile strength [18-20].

Nanoindentation measurements were made on the surface of one sample, which reached the optimal properties in this research, using a mechanical properties microprobe (Agilent G200, USA). Three samples of polished surface were used with six indentation measurements on each sample. A Berkovich diamond tip indenter was used to make low and ultra-low load (5–150 mN) indentations on the selected locations. The displacement of the indenter was continuously monitored and a load-time history of the indentation was recorded. Hardness, H, is defined as the ratio of the maximum applied load, P_{max}, to the projected area of the indented impression, A_c, based on the following equations [14]:

$$H = \frac{P_{max}}{A_c} \quad (1)$$

$$A_c = f\left(h_c^2\right) = 24.5h_c^2 \quad (2)$$

where h_c is the contact depth at the maximum load. According to Oliver-Pharr analysis, the actual depth of contact (h_c) is usually less than the total depth of penetration (h_{max}=displacement measured at maximum load) and a corrected depth of contact is obtained from the following relationship [14]:

$$h_c = h_{max} - \varepsilon\frac{P_{max}}{S} \quad (3)$$

Where ε is a geometrical constant associated with the shape of the indenter (for the Berkowich indenter is a triangular pyramid, ε=0.75) and S is the contact stiffness determined from the initial slope of the unloading curve at P_{max} as follows [14]:

$$S = \left(\frac{dP}{dh}\right)_{h=h_{max}} = \beta\frac{2}{\sqrt{\pi}}E_r\sqrt{A_c} \quad (4)$$

The term β is a constant that depends on the geometry of the indenter and is equal to 1.034 for the Berkovich indenter. E_r is the reduced elastic modulus which defines as the elastic modulus, takes into account the elastic contributions of specimen and the indenter tip as follows [14]:

$$\frac{1}{E_r} = \frac{1-\nu_s^2}{E_s} + \frac{1-\nu_i^2}{E_i} \quad (5)$$

here, E_i and E_s are the respective elastic moduli of the indenter and sample, whereas υ_i and υ_s are the Poisson's ratios of the indenter and the specimen, respectively.

3. Results and discussion

3.1. Densification

Fig. 2 presents the relative density values versus the spark plasma sintering temperature for five titanium samples. Generally, the relative density increased with the SPS temperature from 750 °C to 1200 °C, but, ~1.3% drop was observed at the highest temperature of 1350 °C. It seems that the SPS temperature of 750 °C was not enough to reach a dense material as ~9% porosities were remained after sintering process. Despite the full densification (~99.8%) is achieved at 1200 °C; other samples, which were sintered at 900, 1050 and 1350 °C, have reached ~98% of their theoretical density. The reduction in relative density at

1350 °C seems to be due to the increment of residual fine porosities caused by the grain growth at the highest sintering temperature designated for this research work.

3.2. Phase analysis

XRD patterns of the spark plasma sintered titanium samples, fabricated at 750 °C, 1050 °C and 1350 °C, are shown in Fig. 3. As it can be seen in the spectrum of the sample sintered at 750 °C, the only detectable crystalline phase is titanium (α-Ti), which is similar to that of the as-received Ti powder (Fig. 1b). Therefore, no obvious phase transformation happened after SPS process at 750 °C. Some β-Ti phases were detected by XRD analysis in the samples sintered at 1050 °C and 1350 °C. It seems that the amount of β-Ti increases with sintering temperature, according to the increased intensity/width of the respective peaks. Moreover, the quantitative phase analysis of XRD patterns with the help of *X'pert HighScore Plus* and *Materials Analysis Using Diffraction (MAUD)* software (not presented here) indicated the higher amounts of β-Ti at 1350 °C compared to the lower sintering temperatures. The allotropic transformation of ultra-pure titanium, i.e. the conversion of α-Ti to β-Ti occurs at 882 °C [21]. Despite that, the reverse transformation has not been entirely finalized during the rapid cooling step in SPS process, and hence, some β phases were remained together with α-Ti.

3.3. Microstructure

Microstructural analysis was carried out to study the development of the microstructure and the evolution of the porosity. The representative optical micrographs of the polished surfaces of spark plasma sintered Ti samples are shown in Fig. 4. As it can be clearly observed, two-phase microstructures, containing light "α" grains segregated by intergranular dark "β" layers, were formed in the as-sintered titanium samples.

Since the reverse allotropic transformation has not been totally completed, due to the rapid cooling, some remained β-Ti layers are seen between α-Ti phases. Hence, the microstructure of the samples is composed by α+β lamellae uniformly distributed throughout the microstructure (Fig. 4). Such a phenomenon was slightly occurred in the sample sintered at the temperature of 750 °C which is lower than the allotropic temperature

of 882 °C. As a commercially pure Ti powder (purity> 98%) was used in this work, it seems that the presence of <2% impurities in the starting material may lead to the decreasing of α→β transformation temperature in the as-sintered sample. However, the amount of β-Ti phase (after SPS at 750 °C) was not high enough to be detected by XRD analysis (Fig. 3).

As it can be comparatively seen in Fig. 4, with increasing the SPS temperature, the grains grow significantly. It should be noted that the crystal lattice of β-Ti is body centered cubic (bcc) which has a lower atomic packing factor than that of α-Ti with hexagonal close packed (hcp) structure. Hence, the presence of a less compacted phase assists the diffusion which consequently promotes the grain growth. Microstructure of the sample consolidated at 750 °C (Fig. 4a) is comparatively finer than those sintered at ≥900 °C (Fig. 4b-e). Zadra et al. [12] have also reported an extraordinary grain growth for spark plasma sintered titanium over 900 °C. At sintering temperatures of >900 °C, the self-diffusion coefficient of β-Ti is extremely higher than that of α-Ti [22]. Hence, the growth of β layers is faster than α phases. It should be noted that with increasing the sintering temperature, both α and β layers grow together, but, according to the optical micrographs (Fig. 4), the growth proportion of β-Ti is slightly more.

Fig. 5 shows the microstructure of the sample sintered at 750 ^{0}C, whose characterization was carried out by means of a scanning electron microscope on the cross section of specimens previously ground, polished and etched with Kroll's reactant. As it can be seen, the micrograph of the specimen spark plasma sintered at 750 ^{0}C indicates that such temperature was not high enough to guarantee the complete densification.

3.4. Mechanical properties

Fig. 6 shows the mechanical properties of the spark plasma sintered Ti samples as a function of sintering temperature. The ultimate tensile strength and elongation at break (tensile properties) of samples versus the SPS temperature are reported in Fig. 6a and Fig. 6b, respectively. The worst tensile property belongs to the sample fabricated at the lowest sintering temperature of 750 °C. Ignoring the elongation value at 1050 °C, an obvious trend can be extracted that both ultimate tensile strength and elongation increase with relative

density. To maximize the tensile properties, titanium material has to be spark plasma sintered at 1200 °C. Over this temperature, both tensile properties tend to drop remarkably.

The bending strength curve of titanium samples versus the SPS temperature is displayed in Fig. 6c. As it can be clearly seen in this graph, achieving a bending strength of >2000 MPa is possible by spark plasma sintering at 900-1200 °C. Relatively low bending strengths of the samples sintered at 750 °C and 1350 °C can be related to the high porosity content and fanatic grain growth, respectively.

Fig. 6d displays microhardness test results, precisely $HV_{0.3}$, as a function of the sintering temperature. The sample sintered at 750 °C has a low hardness of 188 HV, may be due to its low relative density value (~91%). In a general manner, hardness increases with SPS temperature up to 1200 °C; but, over this temperature, moderately decreases from 391 to 352 HV (~10% drop). Such a trend was also observed in the relative density curve versus SPS temperature (Fig. 2). Hence, it seems that the hardness strongly depends on the relative density, similar to the trend observed for tensile properties.

The mechanical behavior is due to the compromise between the microstructural evolution, the amount, shape and distribution of the residual porosity and characteristics of the two microstructural features (relative amount of alpha and beta phases) of titanium. In fact, the increase in grain size (growth of alpha and beta layers) and the decrease in relative density of the sample sintered at 1350 °C are two main factors that reduce the tensile and flexural strength of this sample, compared to the specimen sintered at 1200 °C. Moreover, the hardness variations are in agreement with the relative density variations.

Comparing all the mechanical properties measurements, reported in this section, it can be concluded that the optimal sintering temperature for SPS of titanium material is 1200 °C.

3.5. Nanoindentation

Some mechanical properties of the sample sintered at optimal SPS temperature (1200 °C; based on the results discussed in sections 3.1 and 3.4) were characterized by nanoindentation technique. In this way, hardness, elastic modulus and harmonic contact stiffness of α-Ti and β-Ti phases were estimated. Fig. 7 shows the typical load-contact depth curves for α and β phases in the Ti sample spark plasma sintered at 1200 °C. Values

of hardness, elastic modulus and contact stiffness as a function of contact depth for the different phases in Ti sample (sintered at optimal SPS temperature of 1200 °C) are shown in Fig. 8a-c, respectively. The curves of hardness (Fig. 8a) and elastic modulus (Fig. 8b) can be generally divided to two regions, based on the contact depth. In first region (contact depth of <100 nm), the hardness and elastic modulus rapidly increase; however, in second region (contact depth of >100 nm), the elastic modulus almost remains constant but the hardness slightly decreases. For the measurement of hardness, it is required to obtain a fully developed plastic zone by reaching the limiting value of mean contact pressure. Hence, it seems that the primary rise in hardness is due to the elastic contact between indenter tip and the investigated phase and the value of hardness measured under the low applied load cannot reflect the hardness of α-Ti and β-Ti. By obtaining a fully plastic zone, the hardness reaches a plateau. However, fall-off zone in hardness of β phase at higher penetration depths is probably due to the fact that surface roughness is not considered when calculating the hardness value using the Oliver-Phare method based on loading/unloading curves. The incorrect determination of the zero contact point increases the maximum tip penetration depth value at the applied load, and consequently the projected contact area value for the ideal Berkovich tip [23]. In addition, the presence of microscopic pores below the indenter in the investigated area may also decrease the hardness of β-Ti at high penetration depths. Fig. 8c shows an almost linear increase in contact stiffness values in both α and β phases with increase in contact depth. Such an observation can be related to the work-hardening effect as a result of applied indentation load. Li and Bhushan [24] were also reported that the contact stiffness is linearly proportional to the contact depth in the uniform materials with constant elastic modulus. For materials that exhibit strain-hardening, the yield strength effectively increases as its strain increases. Therefore, during the nanoindentation test, the material within the plastic zone becomes harder as the amount of deformation increases which leads to the stiffness increment [16]. In fact, during applying load on the selected phase (α or β), with increased penetration depth and consequently nucleation of dislocation loop, the amount of strain hardening increases, due to the enhanced shear stress required for the expansion and displacement of the dislocation loops by the slip mechanism.

Mechanical properties of existent phases in the Ti sample sintered at 1200 °C, which were separately calculated based on Oliver-Pharr method [14], are presented in Table 2. It should be noted that the indentation loading-unloading curves (Fig. 7) are plotted for different loads, but, the reported values of hardness, elastic modulus and contact stiffness (in Table 2) are their average amounts at the maximum contact depth of 520 nm.

3.6. Fractography

Fig. 9 shows the SEM fractographs of titanium samples spark plasma sintered at different temperatures. The fracture surface of Ti sample sintered at 750 °C (Fig. 9a) exhibits the presence of remarkable large-sized porosities which is consistent with the previously measured value for the relative density of this sample (~9%). It seems that the mass transport phenomenon has slightly transpired even at low SPS temperature; but, incomplete cohesion between the powder particles is clearly seen in this fractograph. This is the reason that such a sample was not able to withstand the mechanical loads and deformations, as discussed in previous sections. Therefore, fabricating a fully dense titanium sample with moderate mechanical properties is not possible at such low sintering temperature.

In other fractographs (Fig. 9b-e), i.e. in the samples spark plasma sintered at temperatures ≥900 °C, well-developed joints between the particles can be definitely observed. The morphology of fracture surface significantly changed with increasing the sintering temperature from 750 °C (Fig. 9a) to 900-1350 °C (Fig. 9b-e). Not only large porosities are not remained after SPS at ≥900 °C, but also a ductile fracture mode with quasi-cleavage areas is seen in the fractographs. The presence of dimples and ripped areas can be attributed to their high plasticity. A laminar morphology is seen in the fractograph of sample sintered at 1350 °C. Zadra et al. [12] explained that the colonies of such plates are responsible for low ductility of titanium when sintered in β phase. This is in consistent with the decreased mechanical properties after SPS at 1350 °C (Fig. 6).

4. Conclusions

Commercially pure titanium samples were spark plasma sintered at different temperatures of 750, 900, 1050, 1200 and 1350 ºC for 5 min under 50 MPa in vacuum. Influences of

sintering temperature on microstructural and mechanical characteristics of spark plasma sintered titanium were investigated. The sample reached only 91% of theoretical density when sintered at 750 ºC with the weakest mechanical properties, compared to other ones. Grain size increased with the SPS temperature, especially above α-Ti to β-Ti transition temperature. Highest relative density of 99.8% and optimal mechanical performances were obtained for the sample sintered at 1200 ºC. This sample was also characterized by nanoindentation technique in order to find and compare the hardness, elastic modulus and contact stiffness of α and β phases.

Acknowledgements

The authors would like to thank Dr. Mojtaba Yazdani in the Dynamic Behavior of Materials Research Laboratory of Sahand University of Technology for his help on evaluation of mechanical properties.

References

[1] Z.H. Zhang, Z.F. Liu, J.F. Lu, X.B. Shen, F.C. Wanga, Y.D. Wang, "The sintering mechanism in spark plasma sintering – Proof of the occurrence of spark discharge," *Scripta Materialia,* vol. 81, p. 56–59, 2014.

[2] M.S. Kumar, P. Chandrasekar, P. Chandramohan, M. Mohanraj, "Characterisation of titanium–titanium boride composites processed by powder metallurgy techniques," *Materials Characterization,* vol. 73, p. 43–51, 2012.

[3] T. Borkar, S. Nag, Y. Ren, J. Tiley, R. Banerjee, "Reactive spark plasma sintering (SPS) of nitride reinforced titanium alloy composites," *Journal of Alloys and Compounds,* vol. 617, p. 933–945, 2014.

[4] L. Ji, B. Chen, S.F. Li, H. Imai, M. Takahashi, K. Kondoh, "Stability of strengthening effect of in situ formed TiCp and TiBw on the elevated temperature strength of (TiCp + TiBw)/Ti composites," *Journal of Alloys and Compounds,* vol. 614, p. 29–34, 2014.

[5] A. Sabahi Namini, S. N. Seyed Gogani, M. Shahedi Asl, K. Farhadi, M. Ghassemi Kakroudi, A. Mohammadzadeh, "Microstructural development and mechanical properties of hot pressed SiC reinforced TiB2 based composite," *International Journal of Refractory Metals and Hard Materials,* vol. 51, p. 169–179, 2015.

[6] R. Chaudhari, R. Bauri, "Reaction mechanism, microstructure and properties of Ti–TiB in situ composite processed by spark plasma sintering," *Materials Science and Engineering A,* vol. 587, p. 161–167, 2013.

[7] Z.H. Zhang, X.B. Shen, S. Wen, J. Luo, S.K. Lee, F.C. Wang, "In situ reaction synthesis of Ti–TiB composites containing high volume fraction of TiB by spark plasma sintering process," *Journal of Alloys and Compounds,* vol. 503, p. 145–150, 2010.

[8] X. Shen, Z. Zhang, S. Wei, F. Wang, S. Lee, "Microstructures and mechanical properties of the in situ

TiB–Ti metal–matrix composites synthesized by spark plasma sintering process," *Journal of Alloys and Compounds,* vol. 509, p. 7692–7696, 2011.

[9] H. Feng, D. Jia, Y. Zhou, "Spark plasma sintering reaction synthesized TiB reinforced titanium matrix composites," *Composites: Part A,* vol. 36 , p. 558–563, 2005.

[10] A. Sabahi Namini, M. Azadbeh, M. Shahedi Asl, "Effect of TiB2 content on the characteristics of spark plasma sintered Ti–TiBw composites," *Advanced Powder Technology,* p. doi:10.1016/j.apt.2017.03.028, 2017.

[11] M. Eriksson, Z. Shen, M. Nygren, "Fast densification and deformation of titanium powder," *Powder Metallurgy,* vol. 48, p. 231–236, 2005.

[12] M. Zadra, F. Casari, L. Girardini, A. Molinari, "Microstructure and mechanical properties of cp-titanium produced by spark plasma sintering," *Powder Metallurgy,* vol. 51, pp. 59-65, 2008.

[13] A. Fischer-Cripps, "Critical review of analysis and interpretation of nanoindentation test data," *Surface & Coatings Technology,* vol. 200 , p. 4153–4165, 2006.

[14] W.C. Oliver, G.M. Pharr, "Measurement of hardness and elastic modulus by instrumented indentation: Advances in understanding and refinements to methodology," *Journal of Materials Research,* vol. 19, pp. 3-20, 2004 .

[15] A.F. Gerday, M.B. Bettaieb, L. Duchêne, N. Clement, H. Diarra, A.M. Habraken, "Material behavior of the hexagonal alpha phase of a titanium alloy identified from nanoindentation tests," *European Journal of Mechanics - A/Solids,* vol. 30, pp. 248-255, 2011.

[16] F.K. Mante, G.R. Baran, B. Lucas, "Nanoindentation studies of titanium single crystals," *Biomaterials,* vol. 20, pp. 1051-1055, 1999.

[17] J. Kwon, M.C. Brandes, P. S. Phani, A.P. Pilchak, Y.F. Gao, E.P. George, G.M. Pharr, M.J. Mills, "Characterization of deformation anisotropies in an α-Ti alloy by nanoindentation and electron microscopy," *Acta Materialia,* vol. 61, pp. 4743-4756, 2016.

[18] C.J. Zhang, F.T. Kong, S.L. Xiao, E.T. Zhao, L.J. Xu, Y.Y. Chen, "Evolution of microstructure and tensile properties of in situ titanium matrix composites with volume fraction of (TiB + TiC) reinforcements," *Materials Science and Engineering A,* vol. 548, p. 152–160, 2012.

[19] L.J. Huang a, L. Geng, H.X. Peng, K. Balasubramaniam, G.S. Wang, "Effects of sintering parameters on the microstructure and tensile properties of in situ TiBw/Ti6Al4V composites with a novel network architecture," *Materials and Desig,* vol. 32 , p. 3347–3353, 2011.

[20] J. Shon, J. Park, K. Cho, J. Hong, N. Park, "Effects of various sintering methods on microstructure and mechanical properties of CP-Ti powder consolidations," *Trans. Nonferrous Met. Soc. China,* vol. 24 , p. 59−67, 2014.

[21] A. Sabahi Namini, M. Azadbeh, M. Shahedi Asl, "Effects of in-situ formed TiB whiskers on microstructure and mechanical properties of spark plasma sintered Ti–B4C and Ti–TiB2 composites," *Scientia Iranica,* p. in press, 2017.

[22] Technical documentary report, "Diffusion in titanium and titanium alloys, No ASD-TDR-62-561,," Armed services technical information agency, Arlington Hall Station, 1962.

[23] G.B. Souza, C.E. Foerster, S.L.R. Silva, C.M. Lepienski, "Nanomechanical properties of rough surfaces," *Materials Research,* vol. 9, pp. 159-163, 2006.

[24] X. Li, B. Bhushan, "A review of nanoindentation continuous stiffness measurement technique and its applications," *Materials Characterization,* vol. 48 , p. 11–36, 2002.

Figures captions:

Fig. 1. (a) SEM micrograph and (b) XRD pattern of as-received commercially pure Ti powder.

Fig. 2. Relative density of the titanium samples spark plasma sintered at different temperatures.

Fig. 3. XRD patterns of Ti samples spark plasma sintered at 750 °C, 1050 °C and 1350 °C.

Fig. 4. Optical microscopy images of the polished surface of titanium samples spark plasma sintered at (a) 750 °C, (b) 900 °C, (c) 1050 °C, (d) 1200 °C and (e) 1350 °C.

Fig. 5. SEM micrograph of the polished surface of titanium sample spark plasma sintered at 750 °C.

Fig. 6. Mechanical properties of the titanium samples as a function of spark plasma sintering temperature: (a) ultimate tensile strength, (b) elongation at break, (c) bending strength and (d) Vickers hardness.

Fig. 7. Indentation loading-unloading curves for α and β phases in the Ti sample sintered at 1200 °C.

Fig. 8. Average values of (a) hardness, (b) elastic modulus and (c) contact stiffness as a function of contact depth for α and β phases in the Ti sample sintered at 1200 °C.

Fig. 9. SEM fractographs of titanium samples spark plasma sintered at (a) 750 °C, (b) 900 °C, (c) 1050 °C, (d) 1200 °C and (e) 1350 °C.

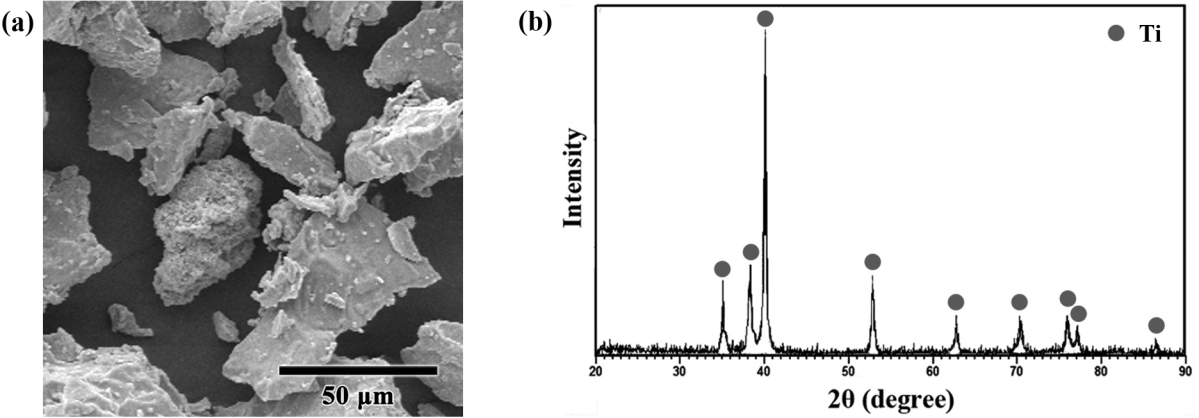
(a)
50 μm
(b)
Ti
Intensity
20
30
40
50
60
70
80
90
2θ (degree)

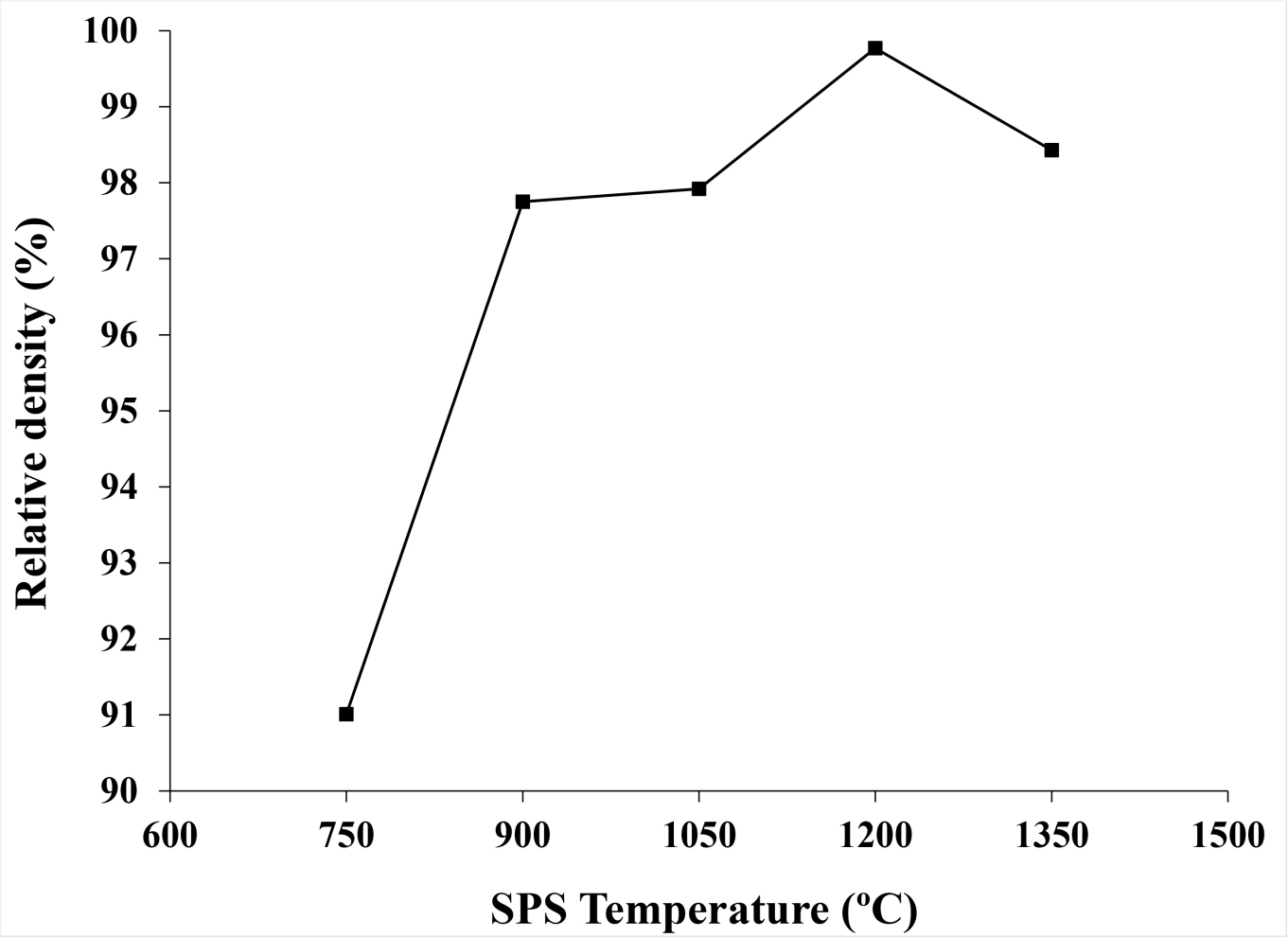
100
99
98
97
96
95
94
93
92
91
90
Relative density (%)
600
750
900
1050
1200
1350
1500
SPS Temperature (°C)

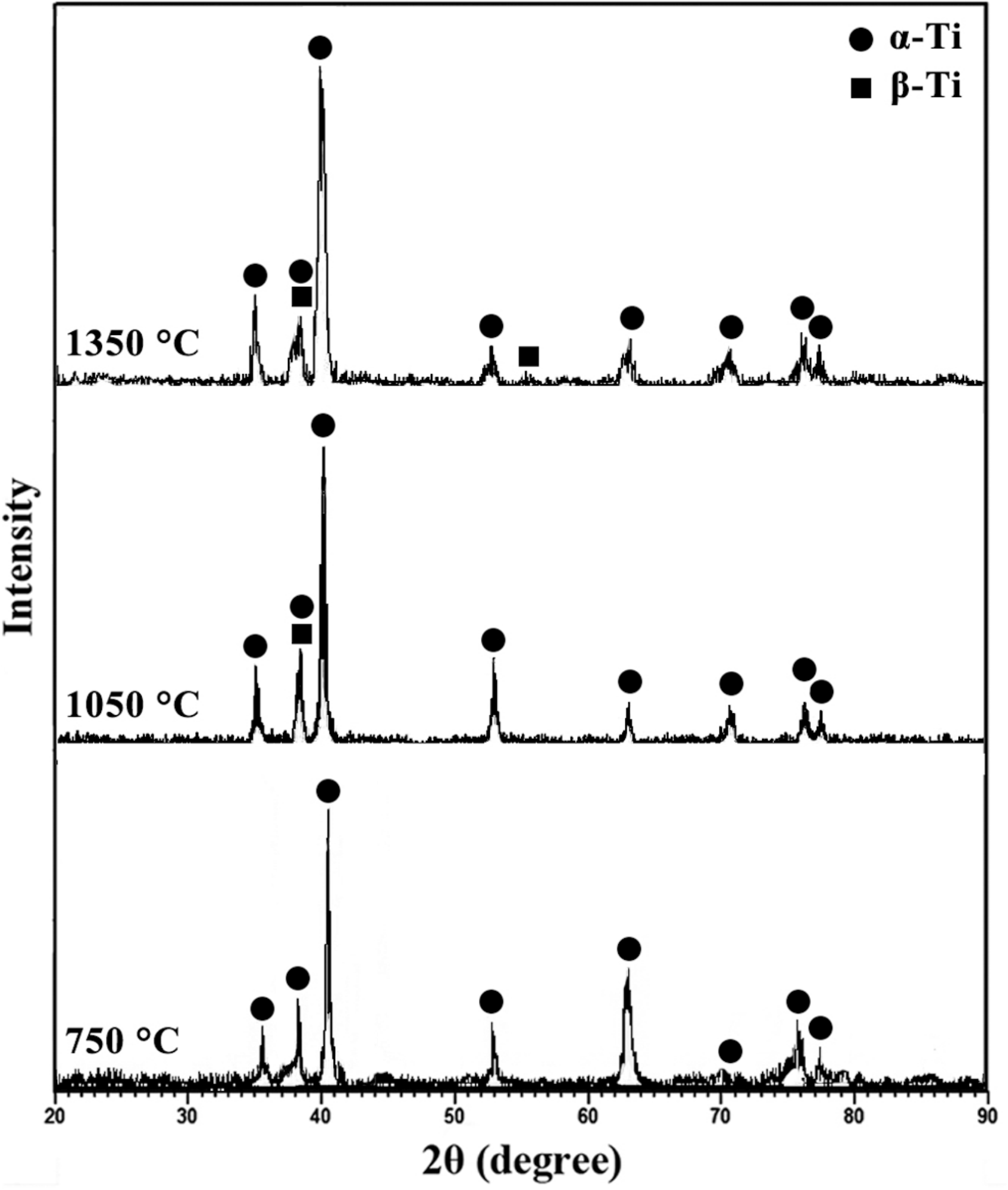
α-Ti
β-Ti
1350 °C
1050 °C
750 °C
Intensity
20
30
40
50
60
70
80
90
2θ (degree)

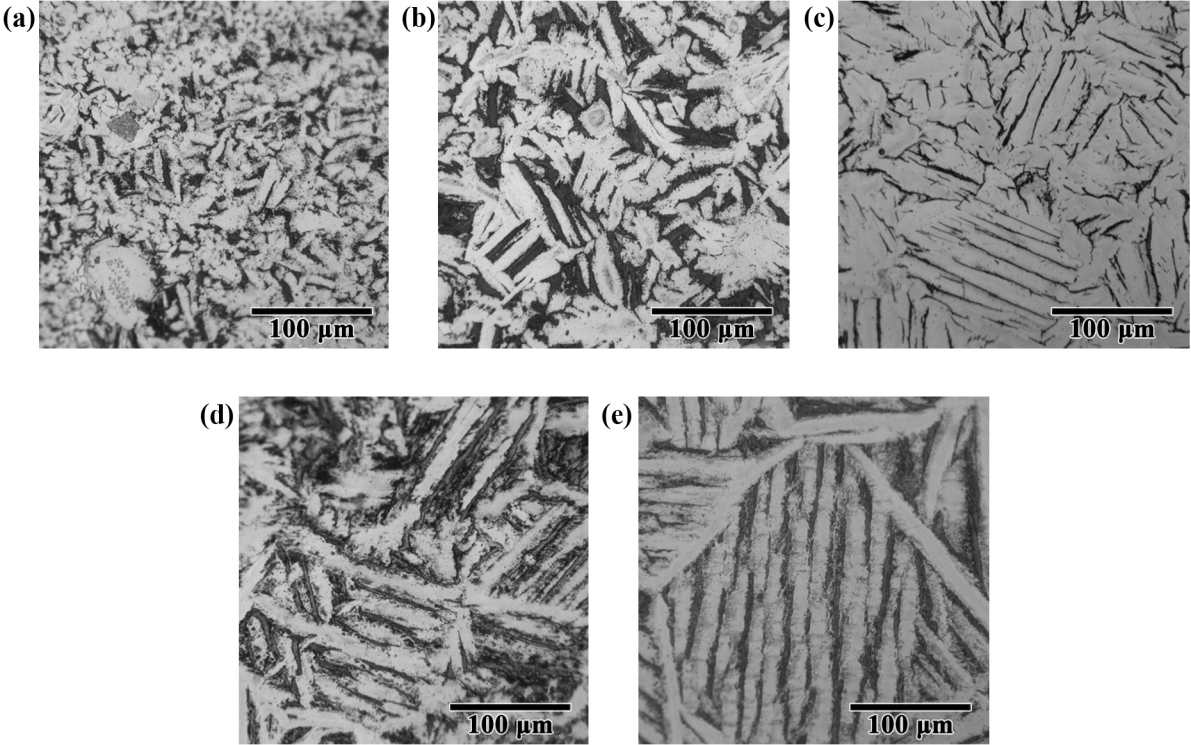
(a)
100 µm
(b)
100 µm
(c)
100 µm
(d)
100 µm
(e)
100 µm

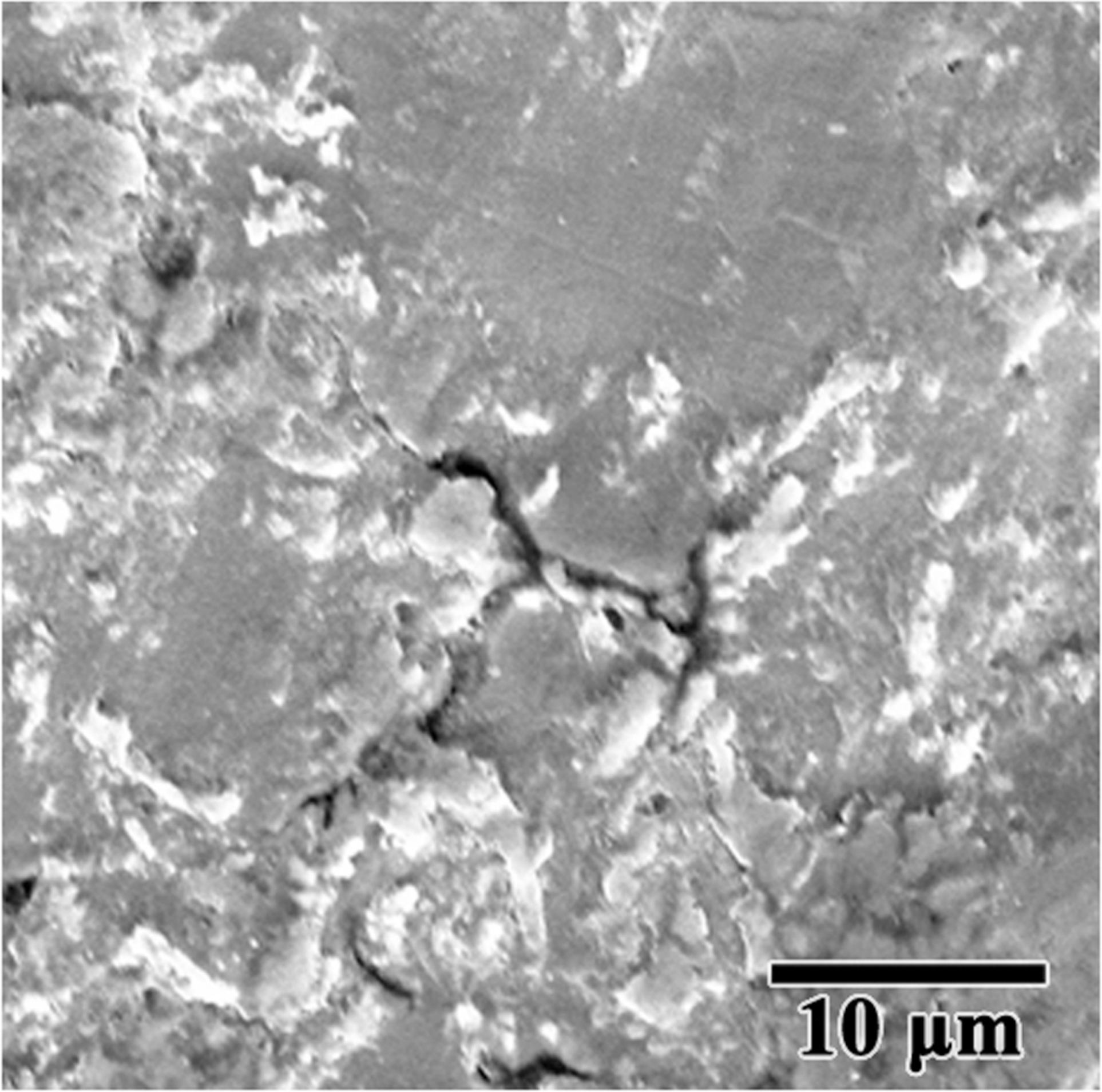
10 µm

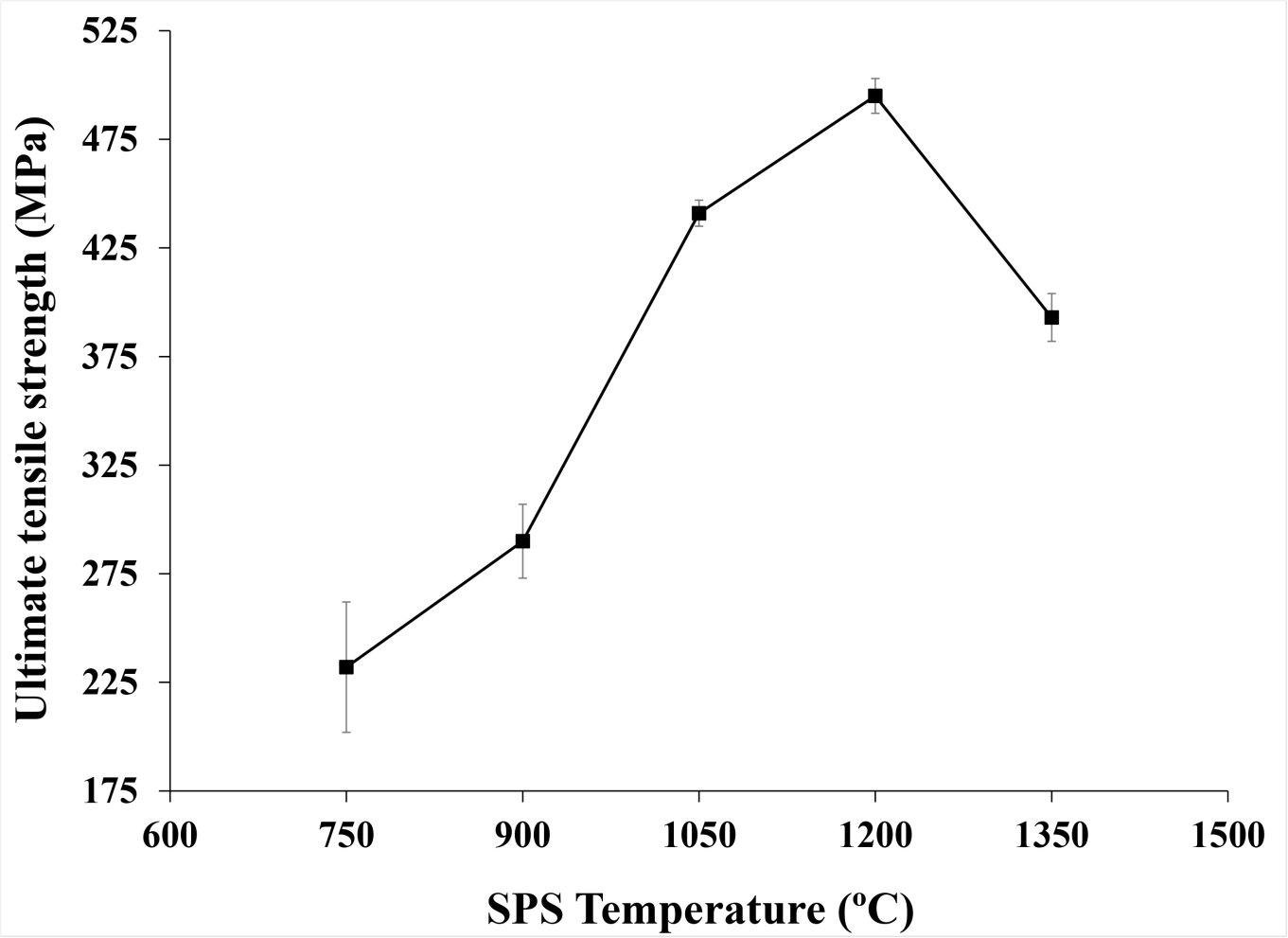
525
475
425
375
325
275
225
175
Ultimate tensile strength (MPa)
600
750
900
1050
1200
1350
1500
SPS Temperature (ºC)

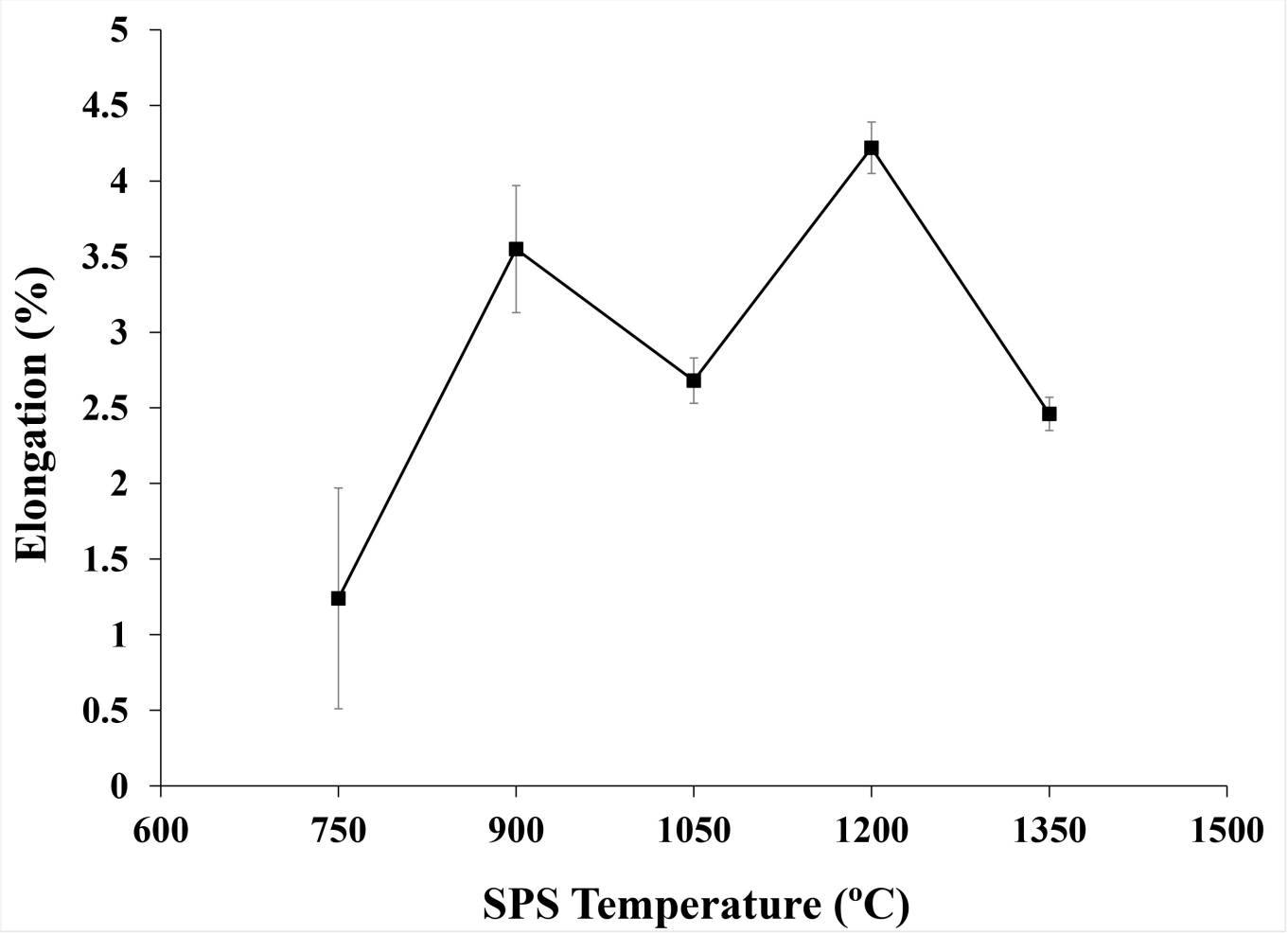
Elongation (%)
5
4.5
4
3.5
3
2.5
2
1.5
1
0.5
0
600
750
900
1050
1200
1350
1500
SPS Temperature (ºC)

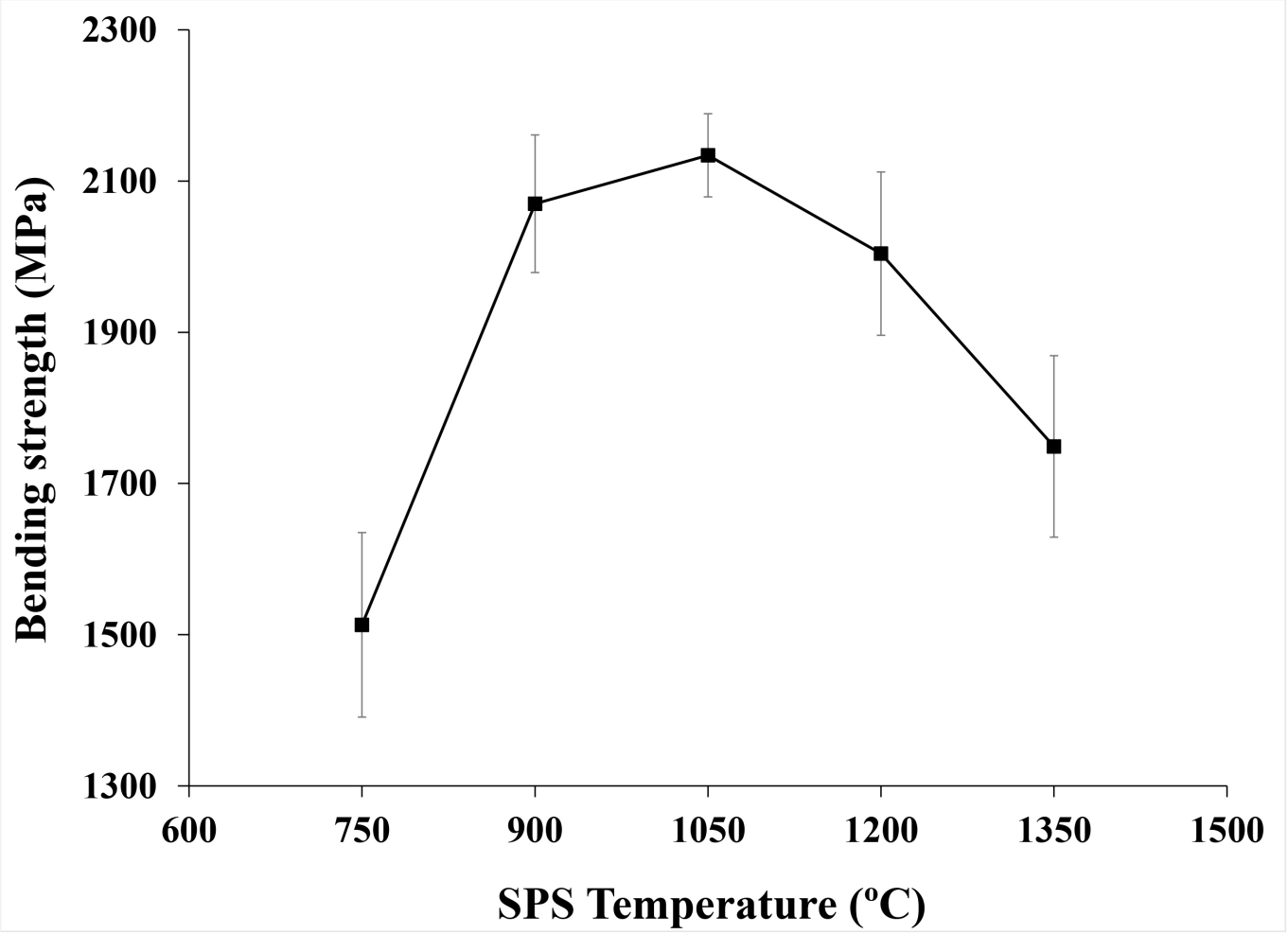
2300
2100
1900
1700
1500
1300
Bending strength (MPa)
600
750
900
1050
1200
1350
1500
SPS Temperature (ºC)

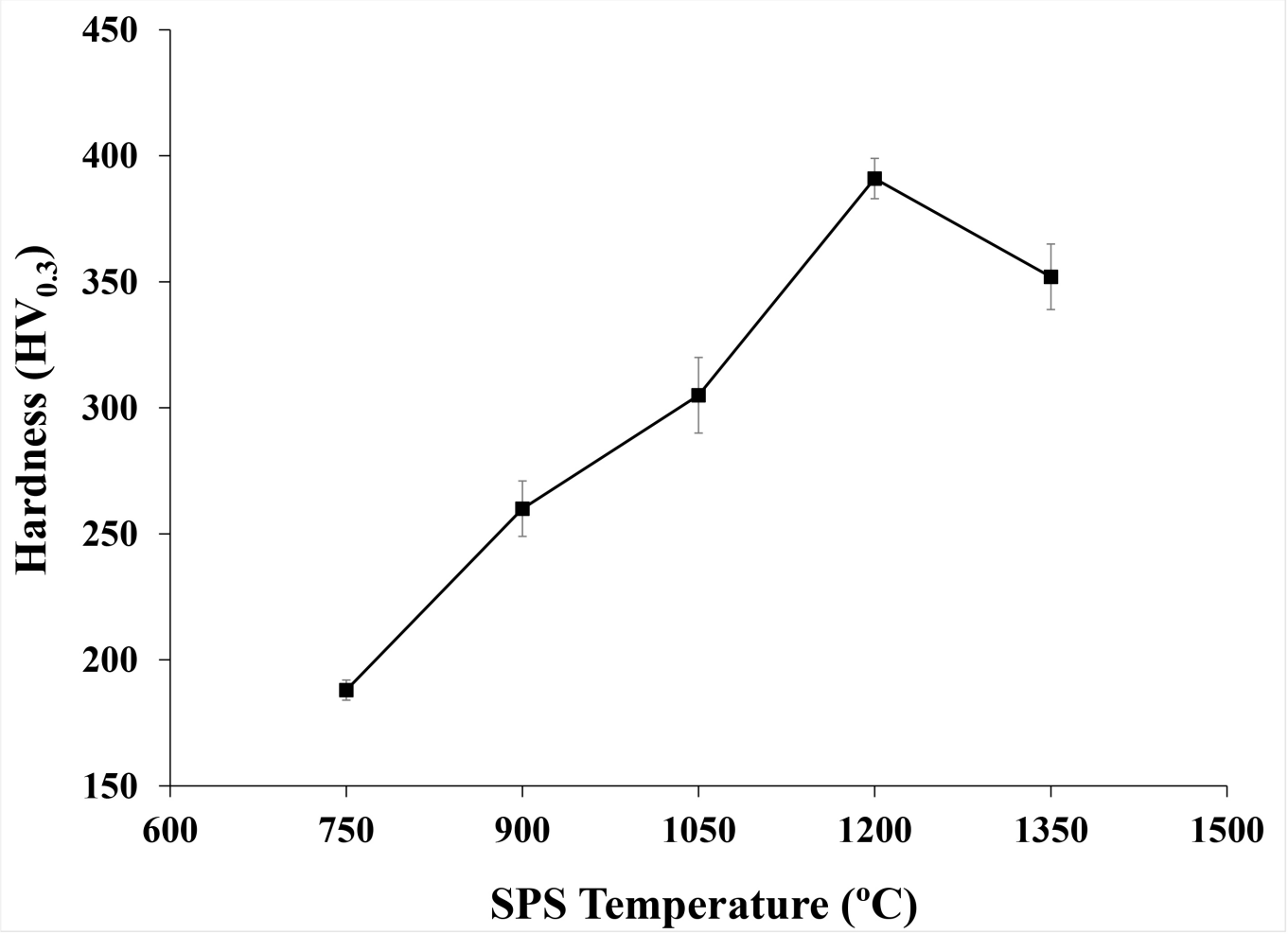
450
400
350
300
250
200
150
Hardness ($HV_{0.3}$)
600
750
900
1050
1200
1350
1500
SPS Temperature (°C)

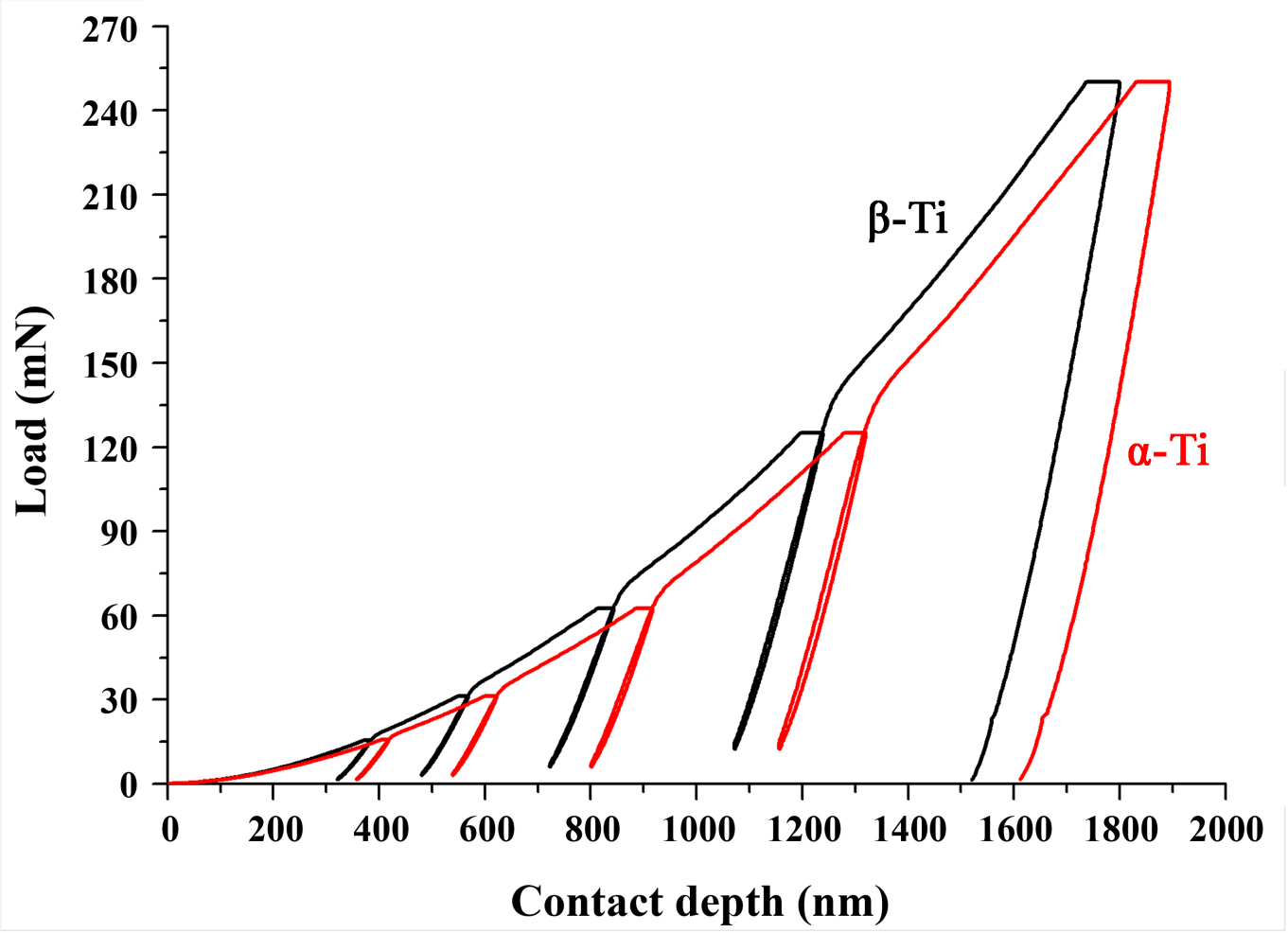
Load (mN)
270
240
210
180
150
120
90
60
30
0
0
200
400
600
800
1000
1200
1400
1600
1800
2000
Contact depth (nm)
β-Ti
α-Ti

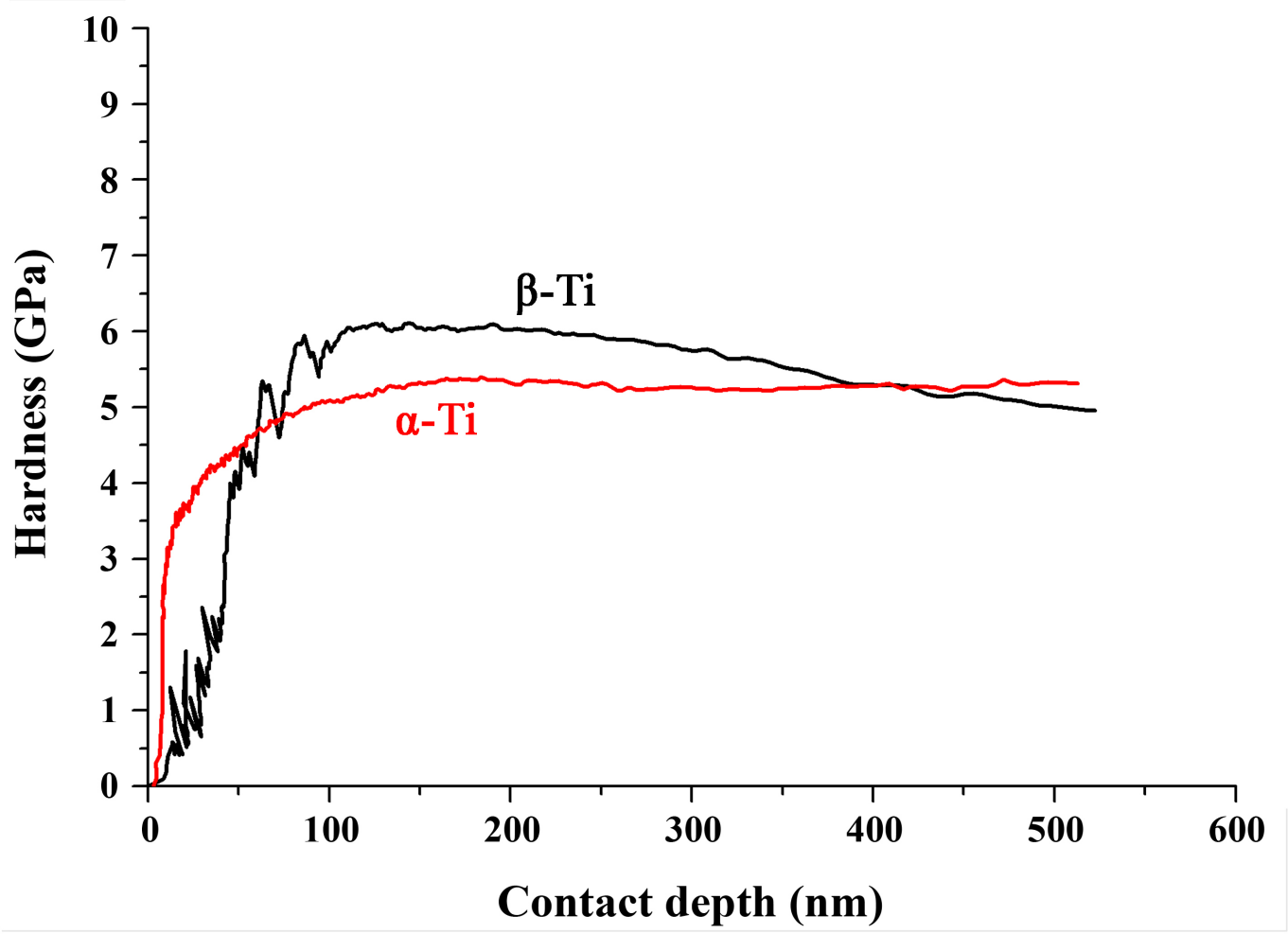
Hardness (GPa)
Contact depth (nm)
β-Ti
α-Ti
0
1
2
3
4
5
6
7
8
9
10
0
100
200
300
400
500
600

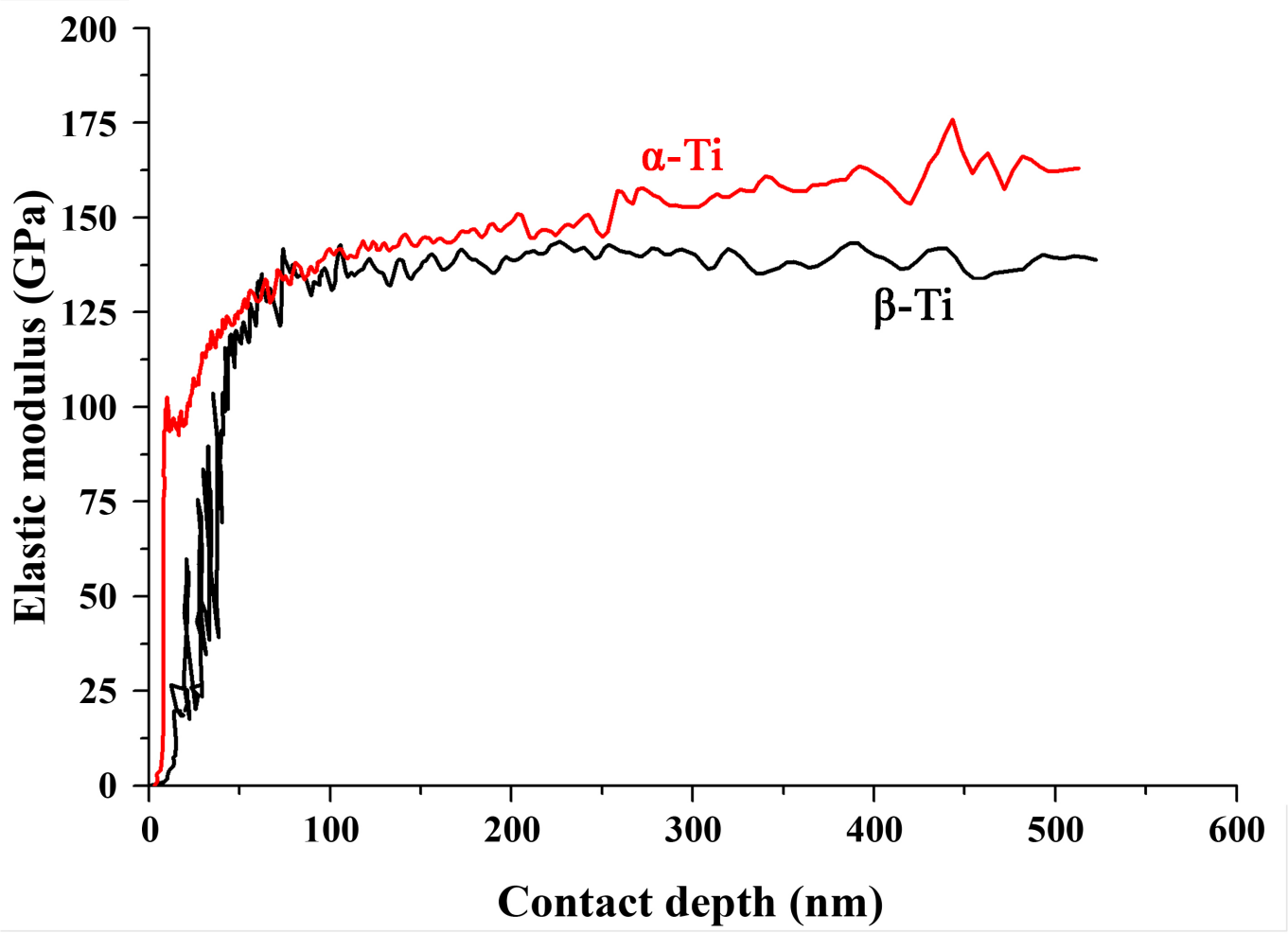
Elastic modulus (GPa)
200
175
150
125
100
75
50
25
0
α-Ti
β-Ti
0
100
200
300
400
500
600
Contact depth (nm)

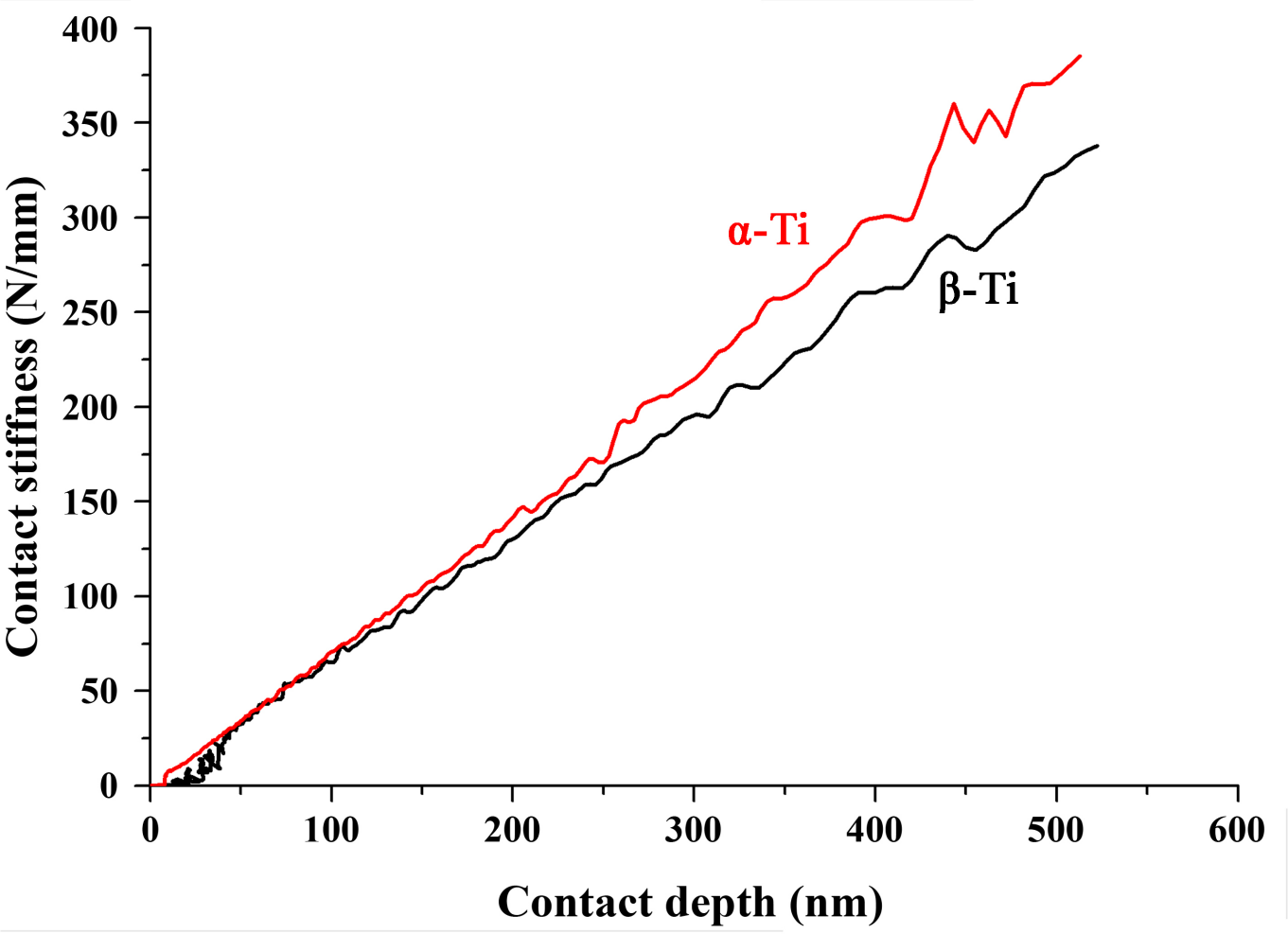
Contact stiffness (N/mm)
400
350
300
250
200
150
100
50
0
0
100
200
300
400
500
600
Contact depth (nm)
α-Ti
β-Ti

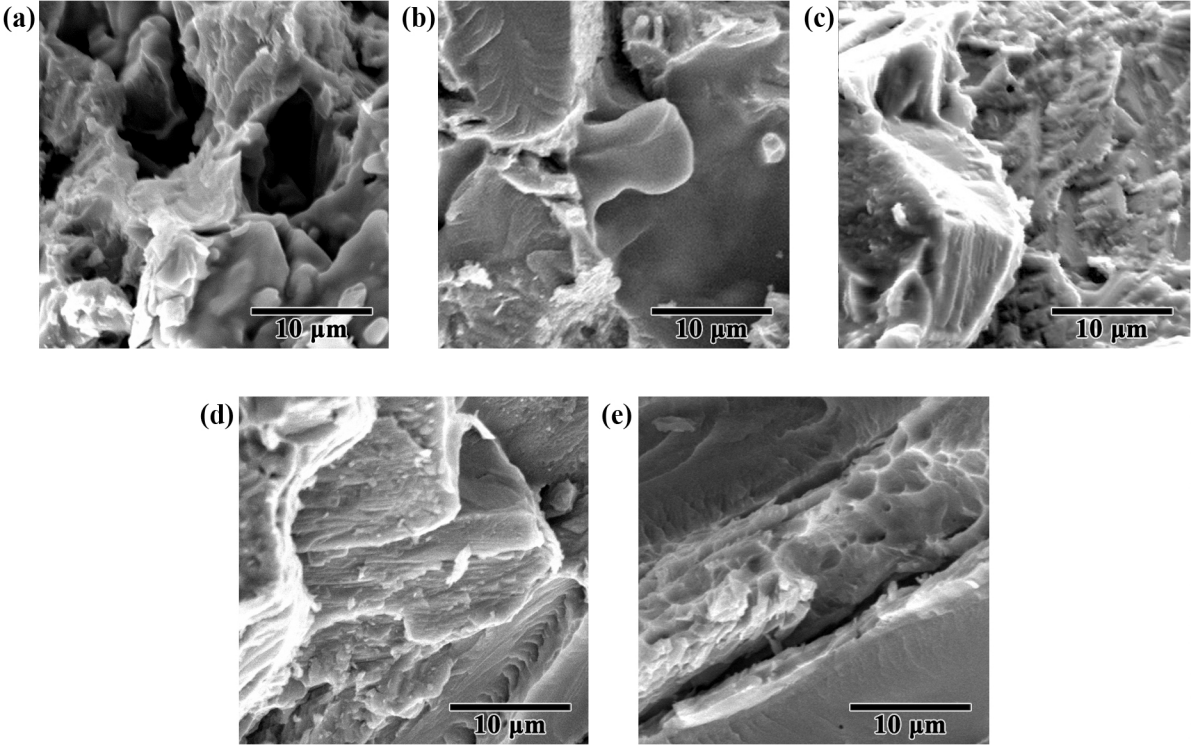
(a)
10 µm
(b)
10 µm
(c)
10 µm
(d)
10 µm
(e)
10 µm

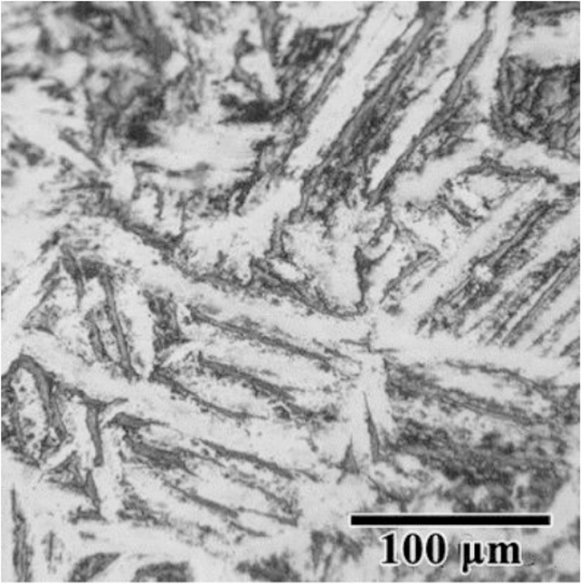
100 µm

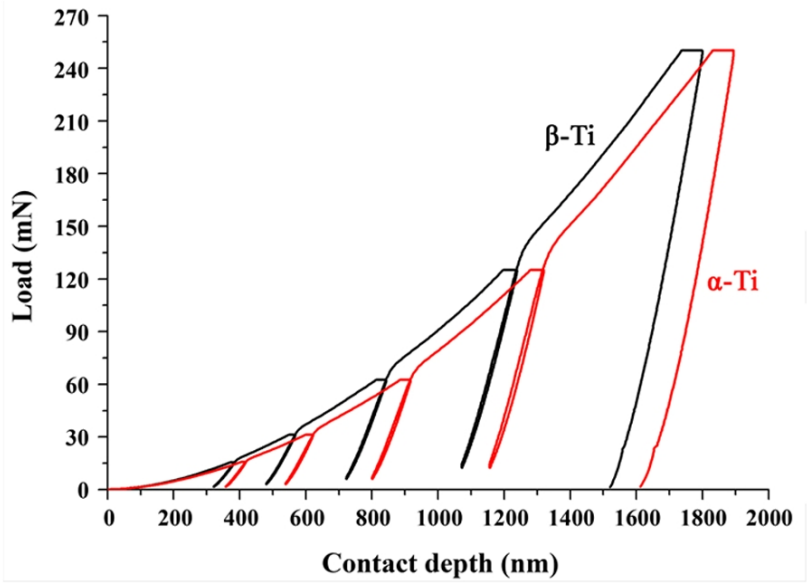
Load (mN)
Contact depth (nm)
β-Ti
α-Ti
0
30
60
90
120
150
180
210
240
270
0
200
400
600
800
1000
1200
1400
1600
1800
2000

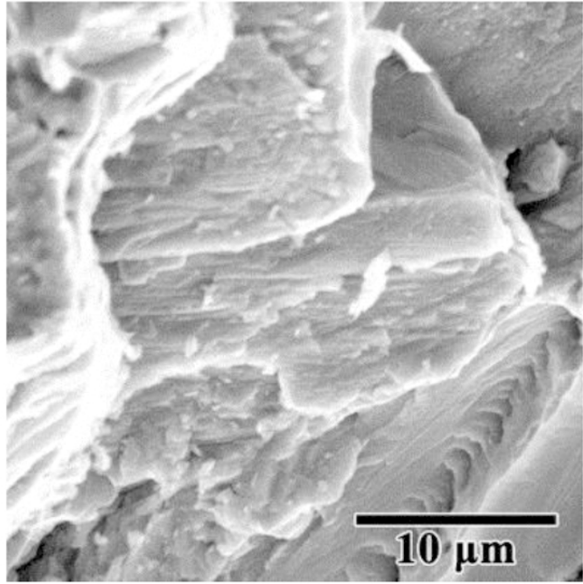
10 µm

Table 1. Chemical composition of as-received Ti powder.

Element	Ti	Fe	Al	V	O	N	H
Content (wt.%)	98.21	0.42	0.23	0.18	0.57	0.09	0.31

Table 2. Nanoindentation results of mechanical properties for different phases of Ti sample sintered at 1200 °C

	α-Ti	**β-Ti**
Hardness (GPa)	5.33	5.68
Elastic modulus (GPa)	147.92	134.32
Stiffness (N/mm)	385	337